488 *Inorg. Chem.* **2010**, *49*, 488–501
DOI: 10.1021/ic901442e

Inorganic Chemistry
Article

Structural Motifs and Biological Studies of New Antimony(III) Iodide Complexes with Thiones

I. Ozturk,[†] S. Filimonova,[†,○] S. K. Hadjikakou,*[,†] N. Kourkoumelis,[‡] V. Dokorou,[§] M. J. Manos,[∥] A. J. Tasiopoulos,[∥] M. M. Barsan,[⊥] I. S. Butler,[⊥] E. R. Milaeva,[○] Jan Balzarini,[#] and N. Hadjiliadis*[,†]

[†]*Section of Inorganic and Analytical Chemistry, Department of Chemistry, University of Ioannina, 45110 Ioannina, Greece,* [‡]*Medical Physics Laboratory, Medical School, University of Ioannina, 45110 Ioannina, Greece,* [§]*X-ray Unit, University of Ioannina, 45110 Ioannina, Greece,* [∥]*Department of Chemistry, University of Cyprus, 1678 Nicosia, Cyprus,* [⊥]*Department of Chemistry, McGill University, 801 Sherbrooke Street West, Montreal, Quebec H2A 2K6, Canada,* [○]*Chemistry Department, M.V. Lomonosov Moscow State University, Leninskie Gory, Moscow, Russia, and* [#]*Katholieke Universiteit Leuven, Rega Institute for Medical Research, Minderbroedersstraat 10, B-3000 Leuven, Belgium*

Received July 22, 2009

Eight new antimony(III) iodide complexes of the heterocyclic thioamides, 2-mercapto-1-methylimidazole (MMI), 2-mercaptobenzimidazole (MBZIM), 5-ethoxy-2-mercaptobenzimidazole (EtMBZIM), 2-mercaptothiazolidine (MTZD), 3-methyl-2-mercaptobenzothiazole (NMeMBZT), 2-mercapto-3,4,5,6-tetrahydropyrimidine (tHPMT), 2-mercaptopyridine (PYT), and 2-mercaptopyrimidine (PMT) of formulas $\{[SbI_3(MMI)_2]\cdot MeOH\}$ (**1**), $[SbI_3(MBZIM)_2]$ (**2**), $\{[SbI_2(\mu_2\text{-I})\text{-}(EtMBZIM)_2]_2\cdot H_2O\}$ (**3**), $[SbI_3(MTZD)]$ (**4**), $[(NMeMBZT)SbI_2(\mu_2\text{-I})_2(\mu_2\text{-S-NMeMBZT})SbI_2$ (NMeMBZT)] (**5**), $\{[SbI_3(tHPMT)_3]\cdot MeOH\}$ (**6**), $[SbI_3(PYT)]$ (**7**), and $[SbI_3(PMT)_2]$ (**8**), have been synthesized and characterized by elemental analysis, FT-IR spectroscopy, FT-Raman spectroscopy, and TG-DTA analysis. The crystal structures of **3**, **4**, **5**, **6**, and **7** were also determined by X-ray diffraction. The complexes show interesting structural motifs. Complex **6** is a monomer, with octahedral (Oh) geometry around the metal ion formed by three sulfur and three iodide atoms. Complexes **3** and **5** are dimers, with a square pyramidal (SP) geometry in each monomeric unit, while complexes **4** and **7** are polymers with pseudotrigonal bipyramidal (ψ-TBP). Two or three sulfur atoms from thioamide ligands and three iodide atoms are bound to Sb atoms forming building blocks for the dimers and polymers. Strong intramolecular interactions between μ_2-I and/or μ_2-S and Sb atoms stabilize both structures. In dimer complex **5**, two terminal iodide and one terminal sulfur atom are bonded to the Sb ion, while two μ_2-I and one μ_2-S bridging atoms bridge the metal ions forming ψ-Oh geometry. Computational studies using multivariant linear regression (MLR) and artificial neural networks (ANN) and considering biological results (50% inhibitory concentration, IC_{50}) as dependent variables derived a theoretical equation for IC_{50} values of the complexes studied. The calculated IC_{50} values are compared satisfactorily with the experimental inhibitory activity of the complexes measured. Complexes **3**−**7** were used to study their influence upon the catalytic peroxidation of linoleic acid by the enzyme Lipoxygenase (**LOX**). Compounds **1**−**8** were also tested for in vitro cytotoxicity, and they showed mostly a moderate cytostatic activity against a variety of tumor cell lines but comparable with those found for the antimony(III) chloride and bromide complexes, reported earlier [Ozturk et al. *Inorg. Chem.* **2007**, *46*, 2861−2866; Ozturk et al. *Inorg. Chem.* **2009**, *48*, 2233−2245].

Introduction

Antimony-based metallotherapeutic drugs have been used in the treatment of leishmania for years as the major therapeutic compounds.[1−5] We have recently shown that antimony(III) chloride or bromide complexes with sulfur donor ligands such as thioamides, also, exhibit antitumor properties.[6−8] Studies on coordination complexes of

*To whom all correspondence should be addressed. E-mail: nhadjis@uoi.gr. Tel.: xx30-26510-08420 (N.H.). E-mail: shadjika@uoi.gr. Tel.: xx30-26510-08374. Fax: xx30-26510-08786 (both).

(1) (a) Yan, S.; Lan, L.; Sun, H. Antimony in Medicine. In *Metallotherapeutic drugs and Metal-based diagnostic Agents−The Use of Metals in Medicine*; Gielen, M., Tiekink, E. R. T., Eds.; Wiley: England, 2005. (b) *Martidale The Extra Pharmacopoeia*, 28th ed.; Raynolds, J. E. F., Ed.; The Pharmaceutical Press: London, 1982.(c) Marsden, P. D. *Rev. Soc. Bras. Med. Trop.* **1985**, *18*, 187–198. (d) Herwaldt, B. L. *Lancet* **1999**, *354*, 1191–1199.
(2) Tiekink, E. R. T. *Crit. Rev. Oncol./Hematol.* **2002**, *42*, 217–224.
(3) Yan, S.; Li, F.; Ding, K.; Sun, H. *J Biol Inorg Chem.* **2003**, *8*, 689–697.
(4) Guo, Z.; Sadler, P. J. *Adv. Inorg. Chem.* **2000**, *49*, 183–306.
(5) Sun, H.; Yan, S. C.; Cheng, W. S. *Eur. J. Biochem.* **2000**, *267*, 5450–5457.
(6) Hadjikakou, S.; Antoniadis, C. D.; Hadjiliadis, N.; Kubicki, M.; Binolis, J.; Karkabounas, S. *Inorg. Chim. Acta* **2005**, *358*, 2861–2866.
(7) Ozturk, I. I.; Hadjikakou, S. K.; Hadjiliadis, N.; Kourkoumelis, N.; Kubicki, M.; Baril, M.; Butler, I. S.; Balzarini, J. *Inorg. Chem.* **2007**, *46*, 8652–8661.
(8) Ozturk, I. I.; Hadjikakou, S. K.; Hadjiliadis, N.; Kourkoumelis, N.; Kubicki, M.; Tasiopoulos, A. J.; Scleiman, H.; Barsan, M. M.; Butler, I. S.; Balzarini, J. *Inorg. Chem.* **2009**, *48*, 2233–2245.

 Published on Web 12/10/2009

antimony(III) are often hindered by the instability of such complexes in aqueous solutions. Significant secondary bonding is also frequently observed in these systems, as a consequence of the M−X σ^* antibonding orbital which has the potential to act as an acceptor orbital toward another donor atom.[9,10] These factors all contribute to the unpredictable structural variations observed for Sb(III) complexes. The reports on structural characterization of antimony(III) triiodide complexes with thione/thiol ligands are rare in the literature. Sulfur containing ligands, such as thiones/thiols,[11−15] thioethers,[16,17] and dithiocarbamates,[18−20] have been used to prepare stable Sb(III) iodide complexes. These include $S(C_6H_4S)_2SbI$,[11] $[\{Sb(k^3\text{-}Tm^{Me})(\mu_2\text{-}I)I\}_2]$ and $[Sb(k^3\text{-}Tm^{Me})\text{-}I(\mu_2\text{-}I)]_2$ (Tm^{Me} = hydrotris(methimazolyl) borate),[12] LSb-(μ-I)2(μ-S)SbL (HL = tetraphenyldithioimidodiphosphine ($SPPh_2NHPPh_2S$)),[13] $SbI(SC_6H_2Me_3\text{-}2,4,6)$,[14] and $S(CH_2\text{-}CH_2S)_2SbI$ and $(CH_2S)_2SbI$.[15] The structures adopted by antimony(III) iodide complexes with thione/thiole, up to now, are pseudotrigonal-bipyramidal,[11,12] (ψ-TBP), square pyramidal (SP),[13,14] and octahedral (Oh)[12,15] (Scheme 1). We have also shown that antimony(III) chloride and antimony-(III) bromide complexes with thione ligands, adopt either pentagonal pyramidal (PP), octahedral (Oh), or square pyramidal (SP) (*trans*-S,*trans*-X or a,b,d-X, *cis*-S,*cis*-X or a, b,c-X or b,c,d-X, X = Cl, Br (Scheme 1)) geometries, and they exhibit selective antiproliferative activity against HeLa cells.[6−8] Generally antimony(III) iodide and chloride complexes are found to be more active than the corresponding bromide complexes.[8] An exception was the polymeric ionic salt $\{[SbBr_5]^{2-}[(PMTH_2^+)_2]\}$ which showed comparable antiproliferative activity against HeLa cells.[8] Since the mechanism of action of Sb complexes is still poorly understood,[6−8] these results prompted us to investigate the correlation between enzyme inhibitions by Sb complexes and their antitumor activity. Lipoxygenase (**LOX**) is an enzyme that takes part in the metabolism of arachidonic acid. LOX catalyzes the oxidation of arachidonic acid to leukotrienes, in an essential mechanism for cell life.[21] Prostaglandines, the final products formed from the metabolism of arachidonic acid, contribute to tumorigenesis acting as angiogenesis factors.[22a] Linoleic acid on the other hand, discovered in beef and dairy products, was proven to be a potential mutagen inhibitor.[22b]

Scheme 1

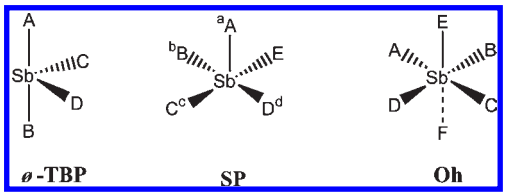

In order to compare the structural and antiproliferative properties of the corresponding antimony(III) iodide derivatives with the same ligands, we report here the new complexes of formulas $\{[SbI_3(MMI)_2]\cdot MeOH\}$ (**1**), $[SbI_3(MBZIM)_2]$ (**2**), $\{[SbI_2(\mu_2\text{-}I)(EtMBZIM)_2]_2\cdot H_2O\}$ (**3**), $[SbI_3(MTZD)]$ (**4**), $[(NMeMBZT)SbI_2(\mu_2\text{-}I)_2(\mu_2\text{-}S\text{-}NMeMBZT)SbI_2$ (NMe-MBZT)] (**5**), $\{[SbI_3(tHPMT)_3]\cdot MeOH\}$ (**6**), $[SbI_3(PYT)]$ (**7**), and $[SbI_3(PMT)_2]$ (**8**) (where MMI = 2-mercapto-1-methylimidazole, MBZIM = 2-mercaptobenzimidazole, EtMBZIM = 5-ethoxy-2-mercaptobenzimidazole, MTZD = 2-mercaptothiazolidine, NMeMBZT = 3-methyl-2-mercaptobenzothiazole, tHPMT = 2-mercapto-3,4,5,6-tetrahydropyrimidine, PYT = 2-mercaptopyridine, and PMT = 2-mercaptopyrimidine[6−8]). These new complexes exhibit interesting structural motifs. Compounds **1**−**8** were finally tested for in vitro cytotoxicity against a variety of tumor cell lines. Complexes **3**−**7** were also used to study their influence upon the catalytic peroxidation of linoleic acid by the enzyme Lipoxygenase (**LOX**).

Results and Discussion

General Aspects. Antimony(III) complexes **1**−**8** have been synthesized by reacting the appropriate thioamide with antimony(III) iodide (SbI_3) in methanolic/acetonitrile solutions, as shown by eqs I−IV. Crystals of complexes **3**−**7**, suitable for X-ray analysis, were grown by slow evaporation of their methanolic/acetonitrile solutions. All complexes prepared are air-stable.

$$n\mathrm{SbI_3} + 2n\mathrm{HL} \xrightarrow{\mathrm{CH_3OH/CH_3CN}} [\mathrm{SbI_3(HL)_2}]_n \quad \begin{matrix} n = 1 \text{ and HL} = \mathrm{MMI}(\mathbf{1}), \\ \mathrm{MBZIM}(\mathbf{2}), \mathrm{PMT}(\mathbf{8}) \\ n = 2 \text{ and HL} = \mathrm{EtMBZIM}(\mathbf{3}) \end{matrix} \qquad \text{(I)}$$

$$\mathrm{SbI_3} + \mathrm{HL} \xrightarrow{\mathrm{CH_3OH/CH_3CN}} [\mathrm{SbI_3(HL)}] \quad \mathrm{HL} = \mathrm{MTZD}(\mathbf{4}), \mathrm{PYT}(\mathbf{7}) \qquad \text{(II)}$$

$$\mathrm{SbI_3} + 3\mathrm{HL} \xrightarrow{\mathrm{CH_3OH/CH_3CN}} [\mathrm{SbI_3(HL)_3}]\cdot\mathrm{MeOH} \quad \mathrm{HL} = \mathrm{tHPMT}(\mathbf{6}) \qquad \text{(III)}$$

$$2\mathrm{SbI_3} + 3\mathrm{HL} \xrightarrow{\mathrm{CH_3OH/CH_3CN}} [(\mathrm{HL})\mathrm{SbI_2}(\mu\text{-}I)_2(\mu\text{-}HL)\mathrm{SbI_2(HL)}] \quad \mathrm{HL} = \mathrm{NMeMBZT}(\mathbf{5}) \qquad \text{(IV)}$$

Thermal Analysis. TG-DTA analysis of complexes **1**−**7** shows one decomposition step, which corresponds to the simultaneous evolution of thione and iodide ligands. An additional step observed in the case of complexes **1**, **3**, and **6** is due to the solvent molecule cocrystallization. The corresponding thermal analysis of **8** consists of two main steps. The first step of decomposition corresponds to the evolution of two ligands and two iodide atoms, while the second one corresponds to an additional iodide atom. Detailed explanations on the decomposition patterns are given in the supplementary information.

(9) Barnes, N. A.; Godfrey, S. M.; Pritchard, R. G.; Ratcliffe, S. *Eur. J. Inorg. Chem.* **2008**, 3661–3667.
(10) Carmalt, C. J.; Norman, N. C. In *Chemistry of Arsenic, Antimony and Bismuth*; Norman, N. C., Ed.; Blackie: London, 1998; Chapter 1.
(11) Alvarado-Rodriguez, J. G.; Andrade-Lopez, N.; Gonzalez-Montiel, S.; Merino, G.; Vela, A. *Eur. J. Inorg. Chem.* **2003**, 3554.
(12) Dodds, C. A.; Reglinski, J.; Spicer, M. D. *Chem.—Eur. J.* **2006**, *12*, 931.
(13) Arca, M.; Garau, A.; Devillanova, F. A.; Isaia, F.; Lippolis, V.; Verani, G.; Abbati, G. L.; Cornia, A. *Z. Anorg. Allg. Chem.* **1999**, *625*, 517.
(14) Peters, M.; Saak, W.; Pohl, S. *Z. Anorg. Allg. Chem.* **1996**, *622*, 2119.
(15) Kociok-Kohn, G.; Molloy, K. C.; Rodriguez-Castro, J. *Inorg. Chem. Commun.* **2008**, *11*, 599.
(16) Pohl, S.; Haase, D.; Peters, M. *Z. Anorg. Allg. Chem.* **1993**, *619*, 727.
(17) Barton, A. J.; Hill, N. J.; Levason, W.; Reid, G. *J. Chem. Soc., Dalton Trans.* **2001**, 1621.
(18) Kello, E.; Kettmann, V.; Garaj, J. *Acta Crystallogr., Sect.C: Cryst. Struct. Commun.* **1985**, *41*, 520.
(19) McKie, G.; Raston, C. L.; Rowbottom, G. L.; White, A. H. *J. Chem. Soc., Dalton Trans.* **1981**, 1360.
(20) Venkatachalam, V.; Ramalingam, K.; Bocelli, G.; Cantoni, A. *Inorg. Chim. Acta* **1997**, *261*, 23.
(21) (a) Samuelsson, B.; Dahlen, S. E.; Lindgren, J.; Rouzer, C. A.; Serhan, C. N. *Science* **1987**, *237*, 1171–1176. (b) Knapp, M. J.; Klinman, J. P. *Biochemistry* **2003**, *42*, 11466–11475.

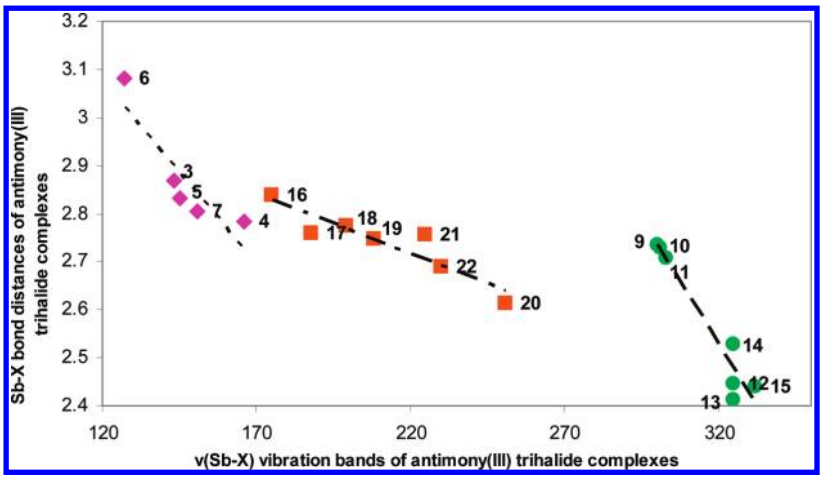

Figure 1. Correlation plot between terminal Sb−X average bond distances (Å) and ν(Sb−X) vibration bands (cm^{-1}) for antimony(III) trihalide−thioamide complexes: (pink diamond) antimony(III) triiodide complexes (**3**−**7**) (this work), (green circle) antimony(III) trichloride complexes[7] {$[SbCl_2(MBZIM)_4]^+ \cdot Cl^- \cdot 2H_2O \cdot (CH_3OH)$} (**9**), $[SbCl_3(tHPMT)_2]$ (**10**), {$[SbCl_2(MBZIM)_4]^+ \cdot Cl^- \cdot 3H_2O \cdot (CH_3CN)$} (**11**), $[SbCl_3(EtMBZIM)_2]$ (**12**), $[SbCl_3(MBZIM)_2]$ (**13**), $[SbCl_3(MTZD)_2]$ (**14**), and $[SbCl_3(NMeMBZT)_2]$ (**15**),[7] (red square) antimony(III) tribromide complexes[8] {$[SbBr_2(\mu_2\text{-Br})(MeMBZIM)_2]_2$} (**16**), {$[SbBr_2(\mu_2\text{-Br})(PYT)_2)_n$} (**17**), {$[SbBr_3(\mu_2\text{-S-tHPMT})(tHPMT)]_n$} (**18**), {$[SbBr_2(MBZIM)_4]^+ \cdot [Br]^- \cdot H_2O$} (**19**), {$[SbBr_2(\mu_2\text{-Br})(EtMBZIM)_2]_2MeOH$} (**20**), {$[SbBr_5]^{2-}[(PMTH_2^+)_2]$} (**21**), and {$[SbBr_2(\mu_2\text{-Br})(MTZD)_2]_n$} (**22**).[8]

Vibrational Spectroscopy. Variations in the geometrical features of Sb(III) halogenate complexes (refs 7, 8, and this work, supplementary information (Figure S1)) results in monomer Oh (**6**), dimers or polymers built up by monomeric units of square pyramidal (SP) (**3**, **5**) or pseudotrigonal-bipyramidal (ψ-TBP) (**4**, **7**) geometries, which also lead to variations in Sb−I and/or Sb−S bond distances due to inter- and intramolecular interactions (see Crystal and Molecular Structures of **3**−**7**). Therefore, far-IR and Raman spectroscopic techniques can be very useful tools in the geometrical characterization of these complexes.

Far-IR spectra of the antimony(III) triiodide complexes **3**−**7** show distinct vibrational bands between 127 and 166 cm^{-1} which are tentatively assigned to ν(Sb−I) vibrations.[23] The ν(Sb−S) vibrational bands are observed between 284 and 330 cm^{-1} [7,8,24] (Table S1). Figure 1 correlates the ν(Sb−X) (X = Cl, Br, I) vibrations observed, versus the average terminal Sb−X bond distances in the complexes (see Crystal and Molecular Structures of **3**−**7** and also refs 7 and 8). Vibrational bands of terminal Sb−I bonds lie at lower wave numbers in the far-IR spectra than the corresponding bands of the terminal Sb−Br and Sb−Cl bonds, indicating lower bond orders for the Sb−I than Sb−Br or Sb−Cl bonds, as expected.

The assignments of the M−L vibrations in complexes **3**−**7** (ν(Sb−I) at 127−166 cm^{-1}, ν(Sb−S) at 284−330 cm^{-1} (Table S1)) were achieved by comparing the far-IR region of all halogen derivatives of the complexes (Figure 1). For complexes **1**, **2**, and **8**, for which no structural data are available, assignments of ν(Sb−I) at 179 (**1**), 143 (**2**), and 170 cm^{-1} (**8**)[23] and ν(Sb−S) vibration bands at 311 (**1**), 270 (**2**), and 290 cm^{-1} (**8**)[7,8,24] have been made.

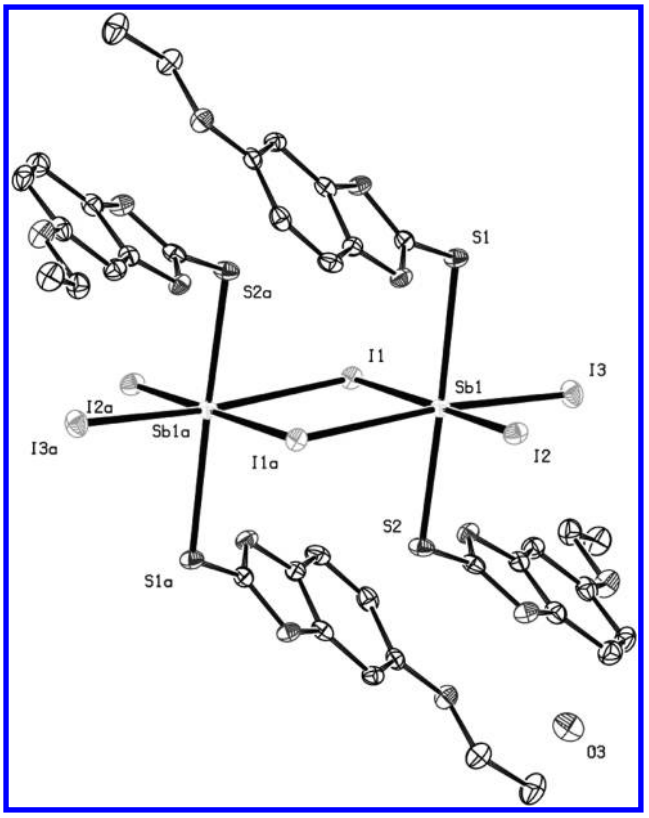

Figure 2. Anisotropic ellipsoid representation of the dimer complex **3** with *trans*-S, *trans*-I square pyramidal (SP) conformation around the metal of each unit. Intermolecular interactions between μ_2-I and Sb atoms finally lead to the dimeric compound with ψ-Oh geometry around the metal center. The ellipsoids are drawn at the 50% probability level. Hydrogen atoms have been omitted for clarity. Symmetry operation to equivalent positions; $a = 2 - x, -y, -z$.

The ν(Sb−S) and ν(Sb−I) stretching vibrations are also Raman active.[7,8,23,25] Although, no direct correlation

(22) (a) Zha, S.; Yegnasubramanian, V.; Nelson, W. G.; Isaacs, W. B.; De Marzo, A. M. *Cancer Lett.* **2004**, *215*, 1–20. (b) Kreich, M.; Claus, P. *Angew. Chem., Int. Ed.* **2005**, *44*, 7800–7804.
(23) Jagodzinski, P. W.; Laane, J. *Raman J Spectros.* **1980**, *9*, 22–27.
(24) Drew, M. G. B.; Kisenyi, J. M.; Willey, G. R.; Wandiga, S. O. *J. Chem. Soc., Dalton Trans.* **1984**, 1717–1721.
(25) (a) Ludwig, C.; Dolny, M.; Gotze, H.-J. *Spectrochim. Acta, Part A* **2000**, *56*, 547–555. (b) Baker, L. J.; Rickard, C. E. F.; Taylor, M. J. *J. Chem. Soc., Dalton Trans.* **1995**, 2895–2899.

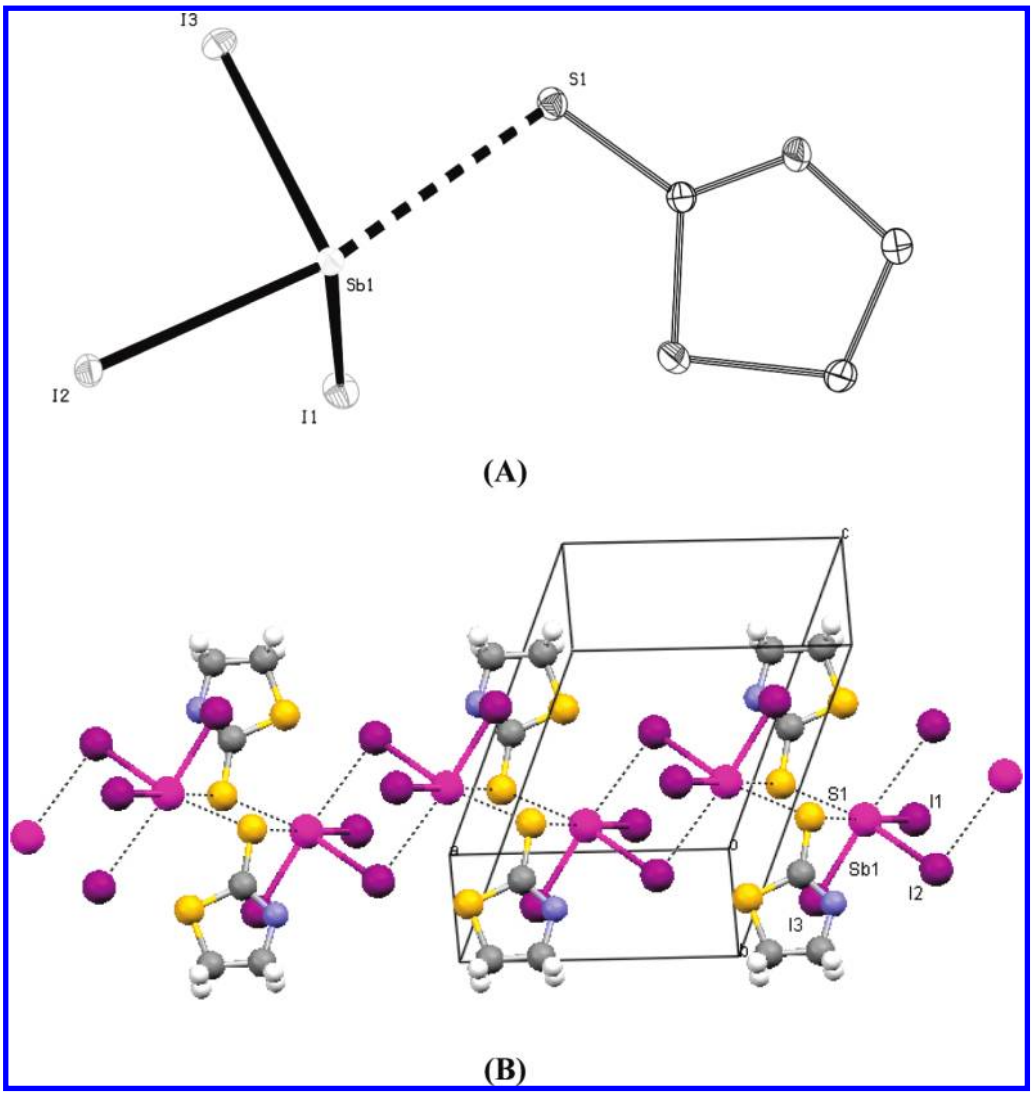

Figure 3. (A) Anisotropic ellipsoid representation of complex **4** with pseutotrigonal-bipyramidal (ψ-TBP) conformation. The ellipsoids are drawn at 50% probability level. Hydrogen atoms have been omitted for clarity. (B) Sequential intramolecular μ_2-S···Sb and μ_2-I···Sb interactions lead to polymerization with ψ-Oh geometry around an Sb center.

between terminal and bridging νSb−I and νSb−S vibrational bands can be made, based on far-IR spectra, Raman spectra show distinct vibrational bands for both,in most cases (see Table S1).

The Raman spectra of the antimony(III) triiodide complexes **3**−**7** show vibrational bands between 190 and 215 cm^{-1} which are assigned to $\nu(Sb-I_{(terminal)})$ vibrations and between 172 and 196 cm^{-1} for the $\nu(Sb-I_{(bridging)})$ bands (Table S1). The $\nu(Sb-S_{(terminal)})$ vibrational bands are observed between 236 and 288 cm^{-1}, while only in case of complex **5** the $\nu(Sb-S_{(bridging)})$ band is observed at 234 cm^{-1} (Table S1). More particularly, the Raman spectrum of the octahedral monomeric complex **6** shows vibrational bands at 190 and 236 cm^{-1}, which are assigned to the ν(Sb−I) and ν(Sb−S), respectively. In dimeric complex **3**, where two terminal iodide and two terminal sulfur atoms are bound to the metal centers, and the ψ-Oh geometry is completed by two μ_2-I bridging atoms, the $\nu(Sb-I_{(terminal)})$ band was observed at 215 cm^{-1} while the $\nu(Sb-I_{(bridging)})$ band at 196 cm^{-1}. The ν(Sb−S) band appears at 253 cm^{-1}. In the dimeric complex **5**, where two terminal iodide and one terminal sulfur atom, are bound to the Sb ion and two μ_2-I and one μ_2-S bridging atoms bridged the metal ions forming ψ-Oh geometry, the $\nu(Sb-I_{(terminal)})$ band appears at 194 cm^{-1}, while the $\nu(Sb-I_{(bridging)})$ band appears at 172 cm^{-1}. The $\nu(Sb-S_{(terminal)})$ and $\nu(Sb-S_{(bridging)})$ bands are observed at 251 and 234 cm^{-1}, respectively. In polymeric complexes **4**, where two terminal iodide atoms and two μ_2-S, two μ_2-I bridging atoms form a ψ-Oh geometry around each of the Sb(III) ions, the $\nu(Sb-I_{(terminal)})$ band is observed at 197 cm^{-1}, while the $\nu(Sb-I_{(bridging)})$ band is at 165 cm^{-1}. The ν(Sb−S) band appears at 288 cm^{-1}, but no $\nu(Sb-S_{(bridging)})$ band was observed. In the case of the polymeric complex **7** where one terminal iodide atom and two μ_2-I bridging atoms form a ψ-Oh geometry around each of the Sb(III) ions, the $\nu(Sb-I_{(terminal)})$ is observed at 179 and the $\nu(Sb-I_{(bridging)})$ band is at 163 cm^{-1}. Complexes **1** and **8** where no structural data are available the ν(Sb−I) bands appear at 193 (**1**) and 179 cm^{-1} (**8**), while ν(Sb−S) vibrational bands are at 247 cm^{-1} (**1**) and 224 and 232 cm^{-1} (**8**), classifying them as either dimeric or polymeric complexes in agreement with the assignment of far-IR spectroscopy.

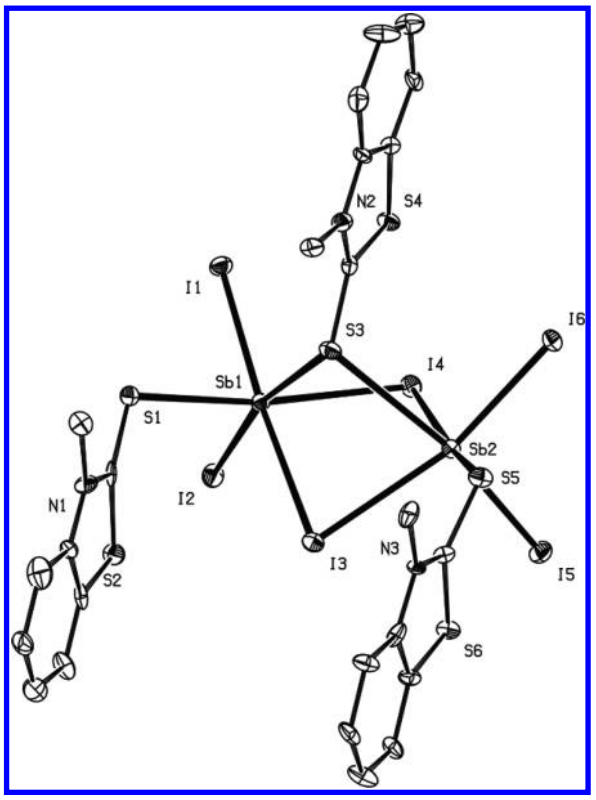

Figure 4. Anisotropic ellipsoid representation of the dimer complex **5** with *trans*-S, *trans*-I square pyramidal (SP) conformation around the metal of each unit. Two μ_2-I···Sb and one μ_2-S···Sb intramolecular interactions finally lead to dimerization with ψ-Oh geometry around the Sb center. The ellipsoids are drawn at the 50% probability level. Hydrogen atoms have been omitted for clarity.

Details on the IR and Raman assignments are given in the supplementary information (Table S1).

Crystal and Molecular Structures of 3−7. Crystal structures of antimony(III) iodide compounds with sulfur containing ligands are very rare in the literature (see the Introduction), and to the best of our knowledge, only six Sb-thione/thiole complexes have been characterized by X-ray diffraction up to now (see the Introduction).

ORTEP diagrams of complexes **3**−**7**, are shown in Figures 2−6, and selected bond lengths and angles are given in Table 1.

Complexes **3** and **5** are dimers (Figures 2 and 4), while complexes **4** and **7** are polymers (Figures 3 and 6). Two or three sulfur atoms from thioamide ligands and three iodide atoms are bound to Sb atoms forming building blocks for the dimers and polymers. The geometry around the metal center in each monomeric unit is either SP (**3**, **5**; Figures 2 and 4) or ψ-TBP (**4**, **7**; Figures 3A and 6A). Strong intramolecular interactions between μ_2-I and/or μ_2-S and Sb atoms lead to dimeric (**3**, **5**; Figures 2 and 4) or to polymeric (**4**, **7**; Figures 3B and 6B) assemblies with ψ-Oh geometries around the Sb(III) ion.

The equatorial plane in both SP units of the dimeric complexes **3** and **5** is formed by two I and two S atoms in a *trans*-S, *trans*-I arrangement. Two terminal iodide (I2−Sb1 = 2.8741(16) and I3−Sb1 = 2.8611(16) Å) and two terminal sulfur atoms (Sb1−S1 = 2.8609(18) and Sb1−S2 = 2.6865(18) Å) are bound to the metal centers in complex **3**, while the ψ-Oh geometry is completed by two μ_2-I bridging atoms (I1−Sb1 = 3.1970(15) and I1−Sb1_a = 3.2295(9) Å). The sum of antimony and iodide van der Waals radii lies between 4.3 and 4.63 Å.[26] However, in dimer

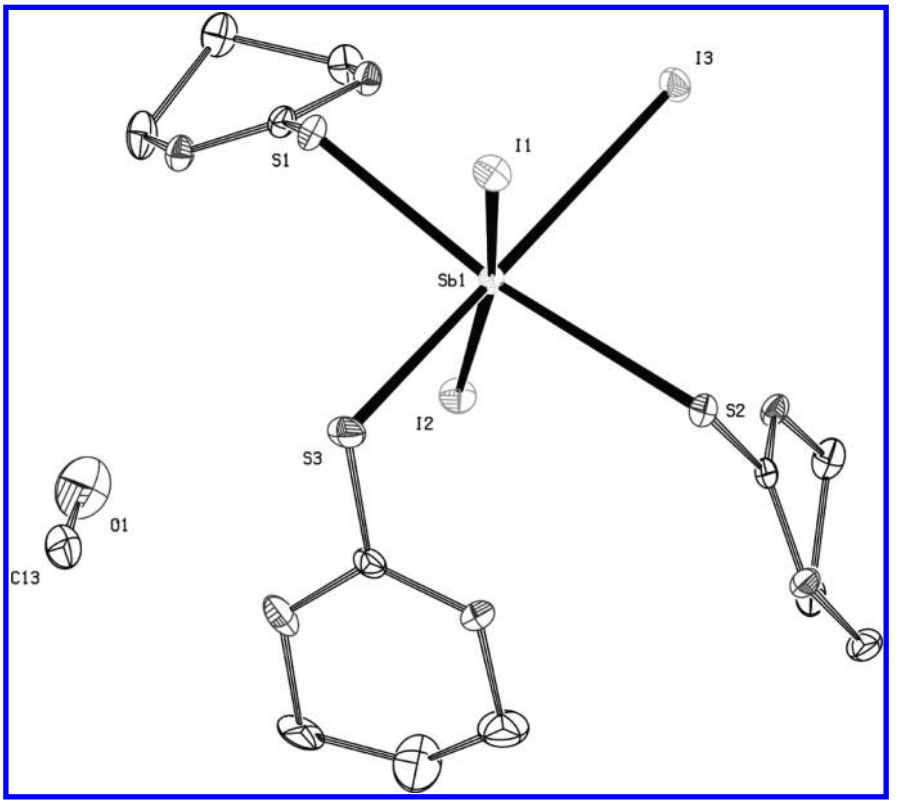

Figure 5. Anisotropic ellipsoid representation of the monomer complex **6** with octahedral (Oh) geometry around the metal ion. A solvent molecule (methanol) is present in the crystal lattice. The ellipsoids are drawn at a 50% probability level. Hydrogen atoms have been omitted for clarity.

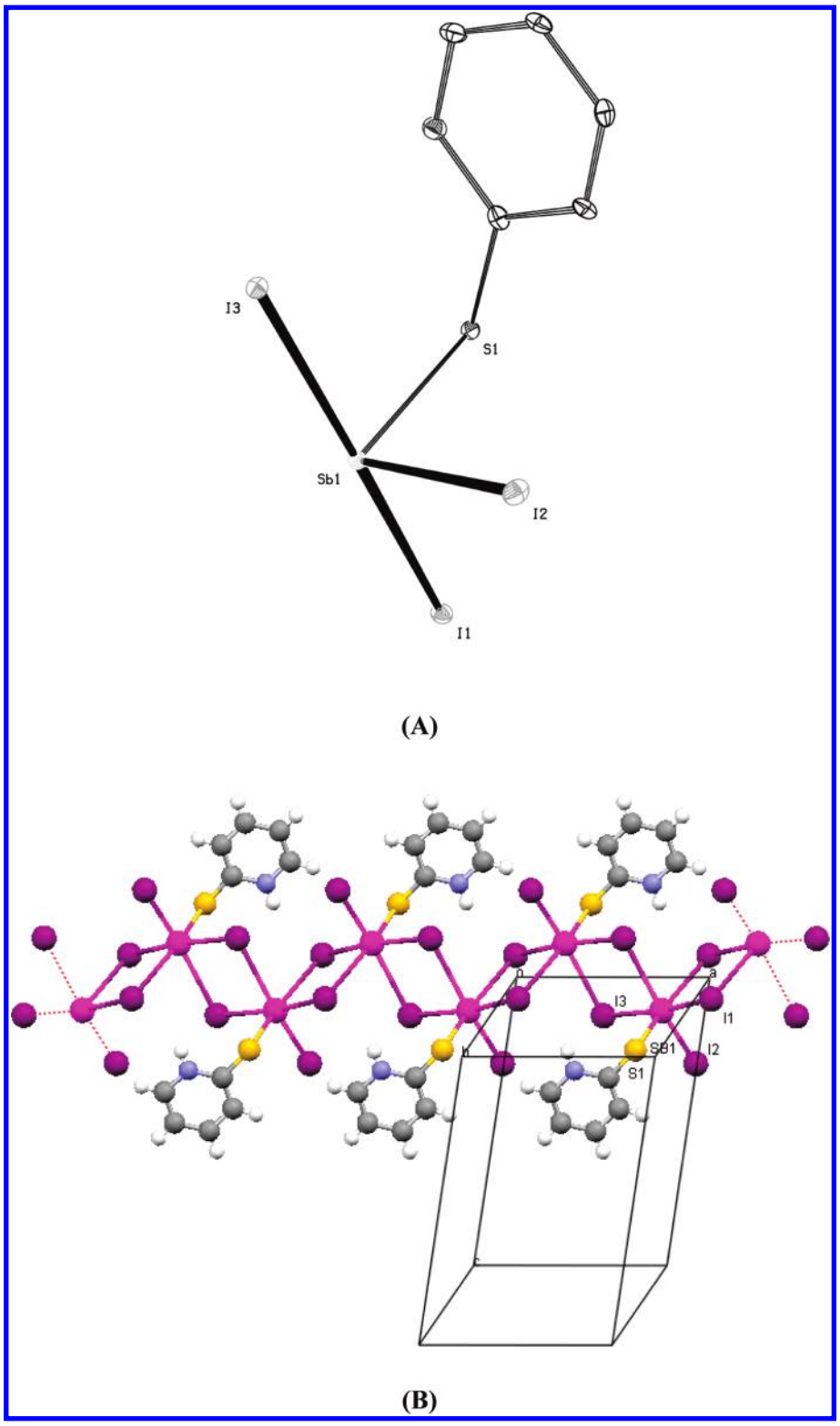

Figure 6. (A) Anisotropic ellipsoid representation of the building block of complex **7** with with pseutotrigonal-bipyramidal (ψ-TBP) conformation. For clarity only one of the two disordered sulfur atoms is shown. The ellipsoids are drawn at the 50% probability level. Hydrogen atoms have been omitted for clarity. (B) Strong intramolecular μ_2-I···Sb interactions lead to 1D polymerization with ψ-Oh geometry around an Sb center.

complex **5**, two terminal iodide (Sb(1)−I(2) = 2.817(3), Sb(1)−I(1) = 2.838(3), Sb(2)−I(5) = 2.800(3), and Sb(2)−I(6) = 2.867(3) Å) and one terminal sulfur atom (Sb(1)−S(1) = 2.754(8) and Sb(2)−S(5) = 2.706(8) Å) are bound to each Sb ion. Two μ_2-I (Sb(1)−I(4) = 3.110(3), Sb(1)−I(3) = 3.230(3), Sb(2)−I(4) = 3.156(3), and Sb(2)−I(3) = 3.195(3) Å) and one μ_2-S (Sb(1)−S(3) = 3.077(9) and Sb(2)−S(3) = 3.118(9) Å), on the other hand, bridge the metal ions forming ψ-Oh geometry.

(26) Batsanov, S. S. *Inorg. Mater.* **2001**, *37*, 871–885. translated from *Neorganicheskie Materialy*, **2001**, *37*, 1031−1046.

Table 1. Selected Bond Lengths (Å) and Angles (deg) for Antimony(III) Iodide Complexes **3**–**7**[a]

complex **3**		complex **4**		complex **5**		complex **6**		complex **7**	
(a) bond lengths		(a) bond lengths		(a) bond lengths		(a) bond lengths		(a) bond lengths	
I1−Sb1	3.1970(15)	Sb(1)−I(3)	2.7767(13)	Sb(1)−S(1)	2.754(8)	Sb(1)−S(1)	2.610(3)	I1−Sb1	3.1231(7)
I1−Sb1_a	3.2295(9)	Sb(1)−I(1)	2.7905(12)	Sb(1)−I(2)	2.817(3)	Sb(1)−S(2)	2.988(3)	I2−Sb1	2.8046(7)
I2−Sb1	2.8742(14)	Sb(1)−I(2)	2.8887(12)	Sb(1)−I(1)	2.838(3)	Sb(1)−S(3)	2.599(3)	I3−Sb1	2.9128(7)
I3−Sb1	2.8611(9)	Sb(1)−S(1)	2.966(4)	Sb(1)−I(4)	3.110(3)	Sb(1)−I(1)	2.9630(10)	Sb1−S1	2.556(3)
Sb1−S1	2.8614(18)	S(1)−C(1)	1.698(13)	Sb(1)−I(3)	3.230(3)	Sb(1)−I(2)	3.0107(10)	Sb1−S1A	2.654(19)
Sb1−S2	2.6868(17)	Sb(1)-S(1a)	3.198(4)	Sb(1)−S(3)	3.077(9)	Sb(1)−I(3)	3.2683(12)	S1−C1	1.738(9)
S1−C10	1.705(4)	Sb(1)-I(2a)	3.5167(14)	Sb(2)−S(3)	3.118(9)	S(1)−C(1)	1.723(10)	S1A-C1	1.52(2)
S2−C1	1.713(4)			Sb(2)−I(5)	2.800(3)	S(2)−C(5)	1.725(10)	Sb1−I1a	3.3655(7)
				Sb(2)−I(6)	2.867(3)	S(3)−C(9)	1.704(11)	Sb1−I3a	3.3889(7)
				Sb(2)−I(4)	3.156(3)				
				Sb(2)−I(3)	3.195(3)				
				Sb(2)−S(5)	2.706(8)				
				S(1)−C(1)	1.65(3)				
				S(5)−C(17)	1.68(3)				
				S(3)−C(9)	1.674(14)				
(b) angles		(b) angles		(b) angles		(b) angles		(b) angles	
I1−Sb1−I2	85.99(2)	I(3)−Sb(1)−I(1)	96.19(4)	S(1)−Sb(1)−I(2)	93.9(2)	S(3)−Sb(1)−S(1)	88.45(12)	I1−Sb1−I2	101.01(2)
I1−Sb1−I3	174.381(10)	I(3)−Sb(1)−I(2)	92.15(3)	S(1)−Sb(1)−I(1)	80.72(19)	S(3)−Sb(1)−I(1)	82.88(8)	I1−Sb1−I3	166.37(2)
I1−Sb1−S1	90.72(2)	I(1)−Sb(1)−I(2)	92.06(4)	I(2)−Sb(1)−I(1)	98.05(9)	S(1)−Sb(1)−I(1)	80.21(6)	I2−Sb1−I3	90.97(2)
I1−Sb1−S2	86.52(2)	I(2)−Sb(1)−S(1)	169.22(8)	S(1)−Sb(1)−I(4)	171.13(19)	S(3)−Sb(1)−I(2)	91.14(8)	I1−Sb1−S1	78.9(2)
S1−Sb1−S2	177.23(3)	I(1)−Sb(1)−S(1)	92.71(8)	I(2)−Sb(1)−I(4)	92.96(8)	S(1)−Sb(1)−I(2)	95.38(6)	I1−Sb1−S1A	80.8(4)
Sb1−I1−Sb1_a	88.03(2)	I(3)−Sb(1)−S(1)	77.73(7)	I(1)−Sb(1)−I(4)	92.74(8)	I(1)−Sb(1)−I(2)	172.63(4)	I2−Sb1−S1	95.64(14)
I1−Sb1−I1_a	91.97(2)			S(1)−Sb(1)−I(3)	97.26(19)	S(2)−Sb(1)−S(3)	91.05(10)	I2−Sb1−S1A	86.6(7)
Sb1_a−I1−Sb1-I3	174.90(1)			I(2)−Sb(1)−I(3)	93.48(8)	S(2)−Sb(1)−S(1)	162.08(7)	I3−Sb1−S1	94.57(6)
				I(1)−Sb(1)−I(3)	168.40(9)	S(2)−Sb(1)−I(3)	88.61(6)	I3−Sb1−S1A	93.5(3)
				I(4)−Sb(1)−I(3)	87.95(7)	S(2)−Sb(1)−I(2)	102.53(5)		
				S(5)−Sb(2)−I(5)	94.3(2)				
				S(5)−Sb(2)−I(6)	82.01(18)				
				I(5)−Sb(2)−I(6)	99.03(9)				
				S(5)−Sb(2)−I(4)	168.9(2)				
				I(5)−Sb(2)−I(4)	95.56(8)				
				I(1)−Sb(1)−S(3)	93.38(4)				
				I(6)−Sb(2)−S(3)	90.90(5)				

[a] Symmetry operations to equivalent positions: **3** (Sb1_a) $2-x, -y, -z$; **4** (Ia) $1-x, 2-y, 1-z$, (S1a) $2-x, 2-y, 1-z$; **5** (S3) $x, 1-y, -^1/_2+z$; **7** (I1a) $-x, -y, -z$, (I3a) $-1-x, -y, -z$.

The geometry around the metal center in each monomeric unit in case of the polymeric complexes **4** and **7** is ψ-TBP (Figures 3A and 6A). In complex **4**, two terminal iodide atoms (Sb(1)−I(3) = 2.7767(13) and Sb(1)−I(1) = 2.7905(12) Å) and sequential two μ_2-S (Sb(1)−S(1) = 2.966(4) and Sb(1)−S(1a) = 3.198(4) Å) two μ_2-I (Sb(1)−I(2) = 2.8887(12) and Sb(1)−I(2a) = 3.5167(14) Å) bridging atoms form a ψ-Oh geometry around each Sb atom leading to a 1D ribbon supramolecular assembly (Figure 3B). In the case of **7**, the ψ-Oh assembly is established by a terminal sulfur (Sb1−S1 = 2.556(3) and Sb1−S1A = 2.654(19) Å) and an iodide (I2−Sb1 = 2.8046(7) Å) atom and μ_2-I bridging atoms (I1−Sb1 = 3.1231(7) and I3−Sb1 = 2.9128(7) Å) leading to 1D polymeric structure (Figure 6B). In complex **7**, there are two disordered sulfur atoms (Table 1).

The Sb−S bond distances varied from 2.568(3) (**7**) to 3.118(9) (**5**) Å (Table 1) in complexes **3**, **4**, **5**, and **7**, with the longest found in **5**. The Sb−S distances in $\{[SbCl_2(MBZIM)_4]^+\cdot Cl^-\cdot 2H_2O\cdot(CH_3OH)\}$, $\{[SbCl_2(MBZIM)_4]^+\cdot Cl^-\cdot 3H_2O\cdot(CH_3CN)\}$, *a*,*b*,*c*-Cl[$SbCl_3$-$(MBZIM)_2$], *a*,*b*,*d*-Cl[$SbCl_3(EtMBZIM)_2$], *a*,*b*,*c*-Cl[$SbCl_3$-$(MTZD)_2$], and *b*,*c*,*d*-Cl[$SbCl_3(tHPMT)_2$][7] varied from 2.48 to 2.85 Å.[11] The Sb−I bond distances in complexes **3**, **4**, **5**, and **7** lie between 2.754(8) (**5**) and 3.5167(14) (**4**) Å (Table 1) with the latest to be the longest such contact measured up to date. The Sb−I bond lengths are in agreement with the corresponding bond distances found in $S(C_6H_4S)_2SbI$ (Sb−I = 2.8603(6) and 2.8747(6) Å),[11] [{Sb(k^3-Tm^{Me})(μ_2-I)I}$_2$] (Sb−$I_{terminal}$ = 3.1498(6) Å) and [Sb(k^3-Tm^{Me})I(μ_2-I)]$_2$ (Tm^{Me} = hydrotris(methimazolyl) borate) (Sb−$I_{terminal}$ = 3.1851(4) and Sb−$I_{bridging}$ = 3.2518(4) Å),[12] LSb(μ-I)2(μ-S)SbL (HL = tetraphenyldithioimidodiphosphine ($SPPh_2NHPPh_2S$)) (Sb(1)−I(1) = 3.2160(8) and Sb(1) = I(1′) 3.1570(8) Å),[13] SbI($SC_6H_2Me_3$-2,4,6) (Sb−I1 = 2.750(1) Å),[14] and $S(CH_2CH_2S)_2SbI$ and $(CH_2S)_2SbI$ (Sb−I = 2.8960(6) Å).[15]

Complex **6**, synthesized in methanol/acetonitrile (1:1) solutions, is a monomeric neutral compound in the solid state, and it is the first example of a neutral Oh geometry of Sb(III) compounds, with meridional conformation (Figure 5). Three sulfur atoms from thione ligands and three iodide ions form an octahedral (Oh) [SbS_3I_3] neutral species, in which the two iodide anions occupy the axial positions. The Sb−I bond distances (Sb(1)−I(1) = 2.9630(10), Sb(1)−I(2) = 3.0107(10), and Sb(1)−I(3) = 3.2683(12) Å) are shorter than the sum of antimony and iodide van der Waals radii (4.3−4.63 Å).[26] The Sb−S bond distances (Sb(1)−S(1) = 2.610(3), Sb(1)−S(2) = 2.988(3), and Sb(1)−S(3) = 2.599(3) Å) are also shorter than the sum of antimony and sulfur van der Waals radii (4.0−4.47 Å).[26] The Sb−S bond distances

Table 2. Cytostatic Activity of the Complexes **1**−**8** against Murine Leukemia (L1210), Murine Mammary Carcinoma (FM3A), Human T-Lymphocyte (Molt4/C8, CEM), and Human Cervix Carcinoma (HeLa) Cells

compound	IC_{50}[a] (μM)					ref
	L1210	FM3A	Molt4/C8	CEM	HeLa	
$\{[SbI_3(MMI)_2]\cdot MeOH\}$ (**1**)	94 ± 74	178 ± 39	58 ± 3	133 ± 42	27 ± 1	b
$[SbI_3(MBZIM)_2]$ (**2**)	104 ± 83	190 ± 18	48 ± 5	120 ± 22	33 ± 7	b
$\{[SbI_2(\mu_2\text{-I})(EtMBZIM)_2]_2\cdot H_2O\}$ (**3**)	39 ± 7	41 ± 34	30 ± 20	46 ± 23	3.2 ± 1.7	b
$[SbI_3(MTZD)]$ (**4**)	46 ± 1	149 ± 95	54 ± 17	127 ± 40	10 ± 6	b
$[(NMeMBZT)SbI_2(\mu_2\text{-I})_2(\mu_2\text{-NMeMBZT})SbI_2(NMeMBZT)]$ (**5**)	18 ± 14	41 ± 11	9.7 ± 2.3	22 ± 2	3.0 ± 1.3	b
$\{[SbI_3(tHPMT)_3]\cdot MeOH\}$ (**6**)	46 ± 8	125 ± 112	38 ± 22	48 ± 40	7.5 ± 0.1	b
$[SbI_3(PYT)]$ (**7**)	35 ± 1	90 ± 71	26 ± 4	58 ± 8	5.2 ± 0.9	b
$[SbI_3(PMT)_2]$ (**8**)	39 ± 3	104 ± 66	31 ± 8	45 ± 12	3.5 ± 1.5	b
$[SbBr_3(TU)_2]$	39 ± 18	91 ± 2	23 ± 4	107 ± 41	23 ± 0	8
$[SbBr_3(MMI)_2]$	71 ± 24	122 ± 2	46 ± 20	127 ± 42	29 ± 3	8
$\{[SbBr_2(MBZIM)_4]^+\cdot[Br]^-\cdot H_2O\}$	42 ± 15	66 ± 1	21 ± 9	67 ± 11	20 ± 2	8
$\{[SbBr_2(\mu_2\text{-Br})(MMBZIM)_2]_2\}$	35 ± 9	75 ± 12	20 ± 3	72 ± 10	20 ± 3	8
$\{[SbBr_2(\mu_2\text{-Br})(EtMBZIM)_2]_2MeOH\}$	52 ± 14	82 ± 3	33 ± 4	54 ± 3	20 ± 0	8
$\{[SbBr_3(\mu_2\text{-S-tHPMT})(tHPMT)]_n\}$	37 ± 10	91 ± 7	27 ± 10	106 ± 34	24 ± 2	8
$\{[SbBr_2(\mu_2\text{-Br})(PYT)_2)_n\}$	33 ± 5	96 ± 10	22 ± 5	72 ± 27	6.3 ± 0.9	8
$\{[SbBr_2(\mu_2\text{-Br})(MTZD)_2]_n\}$	38 ± 13	88 ± 2	25 ± 7	98 ± 18	25 ± 0	8
$[SbBr_3(MMBZT)_2]$	59 ± 39	79 ± 11	21 ± 8	43 ± 23	22 ± 3	8
$\{[SbBr_5]^{2-}[(PMTH_2^+)_2]\}$	20 ± 4	49 ± 5	13 ± 1	59 ± 33	4.2 ± 1.6	8
$\{[SbCl_2(MBZIM)_4]^+\cdot Cl^-\cdot 2H_2O\cdot(CH_3OH)\}$	12 ± 7	36 ± 6	24 ± 16	90 ± 19	6.4 ± 1.6	7, 8
$\{[SbCl_2(MBZIM)_4]^+\cdot Cl^-\cdot 3H_2O\cdot(CH_3CN)\}$	20 ± 15	88 ± 49	30 ± 21	88 ± 5	7.0 ± 2.0	7, 8
$[SbCl_3(MBZIM)_2]$	31 ± 8	103 ± 44	45 ± 33	112 ± 6	7.7 ± 1.2	7, 8
$[SbCl_3(EtMBZIM)_2]$	21 ± 16	41 ± 5	15 ± 10	24 ± 2	6.9 ± 1.1	7, 8
$[SbCl_3(MTZD)_2]$	29 ± 10	56 ± 7	32 ± 22	124 ± 8	6.8 ± 4.4	7, 8
$[SbCl_3(tHPMT)_2]$	29 ± 12	92 ± 55	38 ± 7	118 ± 4	7.7 ± 2.5	7, 8
cisplatin	0.23		0.33		10	7, 8
carboplatin					> 37	7, 8

[a] 50% inhibitory concentration. [b] This work.

found in the Oh ionic $\{[SbX_2(L)_4]X\}$ (X = Cl, Br) complexes lie between 2.73 and 2.79 Å,[7,8] while in the SP neutral $[SbX_3L_2]$ (X = Cl, Br) complexes between 2.48 and 3.01 Å.[7,8]

The C−S bond lengths in the case of complexes **3**−**7** varied from 1.52(2) (**7**) to 1.725(10) (**6**) Å supporting the ligand coordination through their thionate forms (average C−S = 1.69 Å).[7]

In the case of complexes **3** and **5**, the basal I−Sb−I and S−Sb−Sa angles are different than 180°, while the corresponding basal I−Sb−S angles are different than 90°, and therefore, the geometry of their monomeric unit is distorted *trans*-I, *trans*-S SP. This might be due to the lone pair of electrons located on the Sb atom which affects the ideal square pyramidal geometries around the metal ion[27] as expected from the valence shell electron pair repulsion theory (VSEPR) (Table 1).

Biological Tests. Complexes **1**−**8** were evaluated in vitro for their inhibitory activity on the proliferation of murine leukemia cells (L1210), murine mammary carcinoma cells (FM3A), human T-lymphocyte cells (Molt4/C8, CEM), and human cervix carcinoma cells (HeLa). The results of this study are reported, as 50% inhibitory concentration (IC50) values in Table 2. Complexes **1**−**8** showed usually a modest cytostatic activity against the tumor cell lines studied (Table 2). Antimony(III) iodide−thione complexes consistently showed a more selective antiproliferative activity against HeLa cells, which was also observed in the case of the corresponding antimony(III) chloride and bromide complexes studied previously[7,8] (Table 2). However, antimony(III) bromide complexes studied were generally less active than the corresponding chlorides and iodides studied, while antimony(III) chloride complexes show comparable activity with that of the corresponding iodides (Table 2).[7,8] The antiproliferative activity against cervix carcinoma (HeLa) cells of the iodides, in particular compounds **3**−**8**, was 5−6- to > 10-fold more potent than against the murine leukemia and mammary carcinoma and human lymphocyte cells. This selectivity for HeLa cell proliferation is somewhat intriguing but also previously observed for the bromo and chloro derivatives. The HeLa carcinoma cells grew as monolayer cell cultures, whereas the other cell lines were all growing in suspension. Therefore, it may be of interest to investigate the cytostatic activity of the tested compounds against other (solid) tumor monolayer cell lines. The well-known inorganic antitumor drugs cisplatin and carboplatin were rather moderately or poorly inhibitory to HeLa cell proliferation, and thus, the test compounds **3**−**8** were clearly more cytostatic against HeLa cell cultures than cisplatin and carboplatin. Instead, cisplatin was profoundly inhibitory to the L1210 and Molt4/C8 cell proliferation (0.23−0.33 μM). The tested compounds were clearly inferior to cisplatin against these tumor cell lines.

In general, the activity of the complexes against various cell lines seems to increase on passing from monomeric to dimeric or polymeric structures, independent of halogens.

Study of the Peroxidation of Linoleic Acid by the Enzyme Lipoxygenase (LOX) in the Presence of Complexes 3−7. In an attempt to clarify the mechanism of action of Sb(III) complexes prepared, against the tumor cell proliferation, the influence of complexes **3**−**7** on the

(27) (a) Haiduc, I.; Silvestru, C. *Main Group Elements and Their Compounds*; Springer-Verlag: Berlin, 1996; p 355.(b) Liu, Y; Tiekink, E. R. T. *CrystEngCommun* **2005**, *7*, 20–27. (c) Vickaryous, W. J.; Zakharov, L. N.; Johnson, D. W. *Main Group Met. Chem.* **2006**, *5*, 51–59.

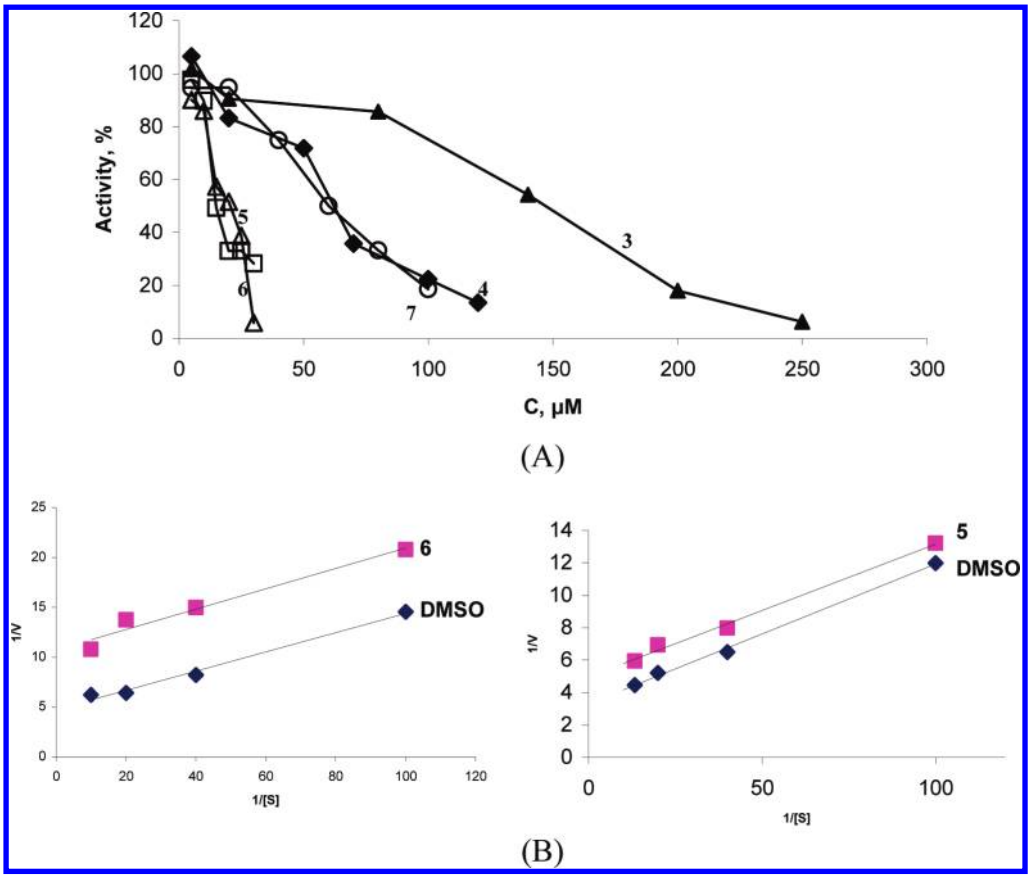

Figure 7. (A) Activity of **LOX** after 10 min of the oxidation of linoleic acid in the presence of complexes **3**−**7**. (B) Grafical ploting for determination of K_m and V_{max} using Lineweaver−Burk coordinates.

oxidation of linoleic acid by the enzyme **LOX** was studied in a wide concentration range. Figure 7A compares the inhibitory effect of complexes **3**−**7** in various concentrations. The degree of LOX activity (A%) in the presence of the complexes was calculated according to

$$A(\%) = \left(\frac{v_0 \text{ in the presence of inhibitor}}{v_0 \text{ in the absence of inhibitor}}\right)100(\%)$$

where v_0 is the initial rate.[28]

The value of the initial rate (v_0, μM min^{-1}) was calculated according to formulas:

$$v_o = \frac{\Delta C}{\Delta t} = \frac{\Delta A}{\Delta t \varepsilon} = \frac{tg\alpha}{\Delta t \varepsilon}$$

where C is the product concentration (hypedroperoxy-linoleic acid), t is the reaction time, ε molar absorbance coefficient of hypedroperoxy-linoleic acid, $tg\alpha$ is the slope of the kinetic curve plotted as absorbance vs time.

The IC_{50} values for **LOX** inhibition were the following: 139.4 (**3**), 67.7 (**4**), 19.2 (**5**), 19.0 (**6**), and 63.4 (**7**) μM, indicating higher inhibitory activity of mer-S,I-{[SbI_3-(tHPMT)$_3$]·MeOH} (**6**). Although Sb(III) complexes **3**−**7** studied inhibit **LOX** activity, their antiproliferative activity does not correspond to the regularity of inhibition of the lipoxygenase activity which was found previously, for tin complexes.[28a−c] This may result in a different mechanism of action of Sb(III) complexes against tumor cell proliferation, as compared to the corresponding Sn(IV) ones.

Table 3. Kinetic Parameters for Complexes **6** and **5**

	6		**5**	
	DMSO (solvent)	complex	DMSO (solvent)	complex
K_m, mmol L^{-1}	0.020	0.009	0.026	0.016
V_{max}, mmol L^{-1} s^{-1}	21.0	9.3	30.3	20.1

The inhibition type caused by the complexes **5** and **6**, with the higher inhibitory activity, was studied by steady-state kinetics. For this, a series of experiments were performed in order to determine the reversibility of inhibition. The reversible type of inhibition was tested by incubating the substrate with the inhibitor before adding the enzyme at different periods of time (from 1 to 10 min). The incubating time showed no influence on enzyme activity in the presence of constant complex concentration, suggesting a reversible type of inhibition. The kinetic parameters (K_m and V_{max}) of complexes **5** and **6** were evaluated by performing a series of experiments with various substrate concentrations in the presence and in the absence of the complexes. The experimental data

(28) (a) Abdellah, M. A.; Hadjikakou, S. K.; Hadjiliadis, N.; Kubicki, M.; Bakas, T.; Kourkoumelis, N.; Simos, Y. V.; Karkabounas, S.; Barsan, M. M.; Butler, I. S. *Bioinorg. Chem. Appl.* **2009**542979. (b) Balas, V. I.; Hadjikakou, S. K.; Hadjiliadis, N.; Kourkoumelis, N.; Light, M. E.; Hursthouse, M.; Metsios, A. K.; Karkabounas, S. *Bioinorg. Chem. Appl.* **2008**654137. (c) Xanthopoulou, M. N.; Hadjikakou, S. K.; Hadjiliadis, N.; Kubicki, M.; Karkabounas, S.; Charalabopoulos, K.; Kourkoumelis, N.; Bakas, T. *J. Organomet. Chem.* **2006**, *691*, 1780–1789. (d) Segel, I. H. *Biochemical Calculations*, 2nd ed.; J. Wiley & Sons Inc.: New York, 1976.

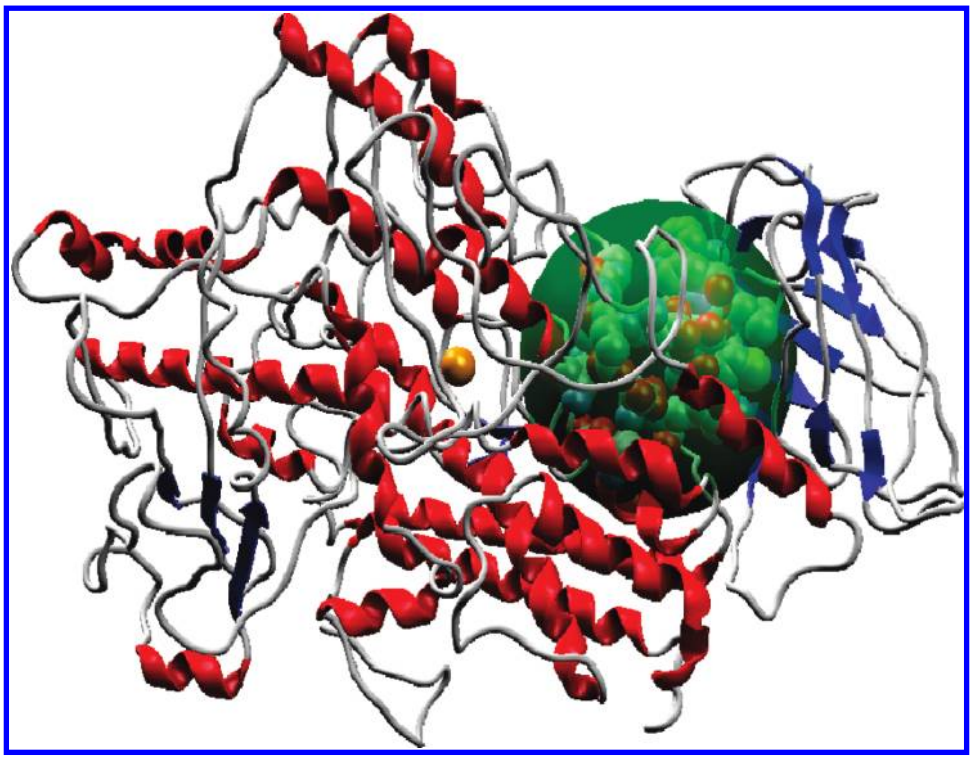

Figure 8. Binding pocket of the complexes **3**−**7**.[29a]

were processed by graphical methods in Lineweaver−Burk coordinates (double reciprocal method). The K_m and V_{max} values were estimated from the slope and intercept of the line and are shown in Table 3. Control experiments, using solvent instead of inhibitor, were performed for each complex. Concentrations of 12 and 15 μM were used for **5** and **6** complexes, respectively. The experimental data plotting for complexes **5** and **6** are shown in Figure 7B. For both complexes, the curves of reaction with and without inhibitor are parallel. Thus, the compounds studied inhibit the enzyme with an uncompetitive inhibition mechanism.[28d] In this mechanism, the **EI** (enzyme−inhibitor) is not formed, but only the **ESI** (enzyme−substrate−inhibitor) (Scheme 2).[28d] This occurs when the inhibitor binds to a site which only becomes available following the substrate (S) bound to the active site of the enzyme.[28d] This further supports our suggestion for a different mechanism of action of Sb(III) complexes against tumor cell proliferation, as compared to the corresponding Sn(IV) ones which act through a mixed inhibition mechanism.[28a−c]

Computational Methods—Docking Study. The inhibitory effectiveness of a compound on a receptor can be evaluated by a docking process and by exploring the interaction between the compound and the receptor. All complexes were docked into the same vicinity of the protein consisting of the larger hydrophobic pocket (Figure 8).[29a] There does not seem to be any constant binding orientation of the compounds in this binding pocket. All but **4** complexes show hydrogen bonding interactions among the ring N atom and the amino acid residue ASP768 as expected since iodide is less electronegative than N atoms. It is noted that the iodides were not removed for the calculations. Furthermore, there are hydrogen bondings linking N atoms and THR529 and GLU78. Significant steric interactions between the ligands and the protein were assigned and calculated using the piecewise linear potential (PLP).[29b,c] A positive correlation (R^2 = 0.98; slope = 1.73 ± 0.08) is found between the steric effect and the binding affinity of the ligands (Figure 9A). This is probably due to the importance of the hydrophobic surface of the molecules. Relatively small surfaces and small steric interactions are responsible for poor binding and vice versa.[30a] Although this binding area is also found to be the binding pocket of organotin complexes docked, causing strong enzyme inhibition,[28a−c] the lower such activity of Sb(III) thione complexes studied here is most probably due to the different mechanism of enzyme inhibition toward organotins (uncompetitive in case of Sb(III) complexes contrary to mixed mechanism of organotin complexes (see above)).

Table 4 summarizes the binding energies (E) when the substrate (S, linoleic acid) binds in the enzyme **LOX** (**E**) for the formation of ES complex (E = −100.25 kJ/mol)

(29) (a) Thomsen, R.; Christensen, M. H. *J. Med. Chem.* **2006**, *49*(11), 3315–3321. (b) Gehlhaar, D. K.; Verkhivker, G.; Rejto, P. A.; Fogel, D. B.; Fogel, L. J.; Freer, S. T. Docking Conformationally Flexible Small Molecules Into a Protein Binding Site Through Evolutionary Programming. *Proceedings of the Fourth International Conference on Evolutionary Programming*, 4th Conference, San Diego, CA, USA, March 1−3, 1995; pp 615−627. (c) Gehlhaar, D. K.; Bouzida, D.; Rejto, P. A. Fully Automated And Rapid Flexible Docking of Inhibitors Covalently Bound to Serine Proteases. *Proceedings of the Seventh International Conference on Evolutionary Programming*, 7th Conference, Ep98, San Diego, CA, USA, March 25−27, 1998; pp 449−461.

(30) (a) Setzer, W. N. *J. Mol. Model.* **2008**, *14*, 967–973. (b) Halperin, I.; Ma, B.; Wolfson, H.; Nussinov, R. *PROTEINS: Struct., Funct., Genet.* **2002**, *47*, 409–443. (c) Xanthopoulou, M. N.; Hadjikakou, S. K.; Hadjiliadis, N.; Milaeva, E. R.; Gracheva, J. A.; Tyurin, V. Y.; Kourkoumelis, N.; Christoforidis, K. C.; Metsios, A. K.; Karkabounas, S.; Charalabopoulos, K. *Eur. J. Med. Chem.* **2008**, *43*, 327–335.

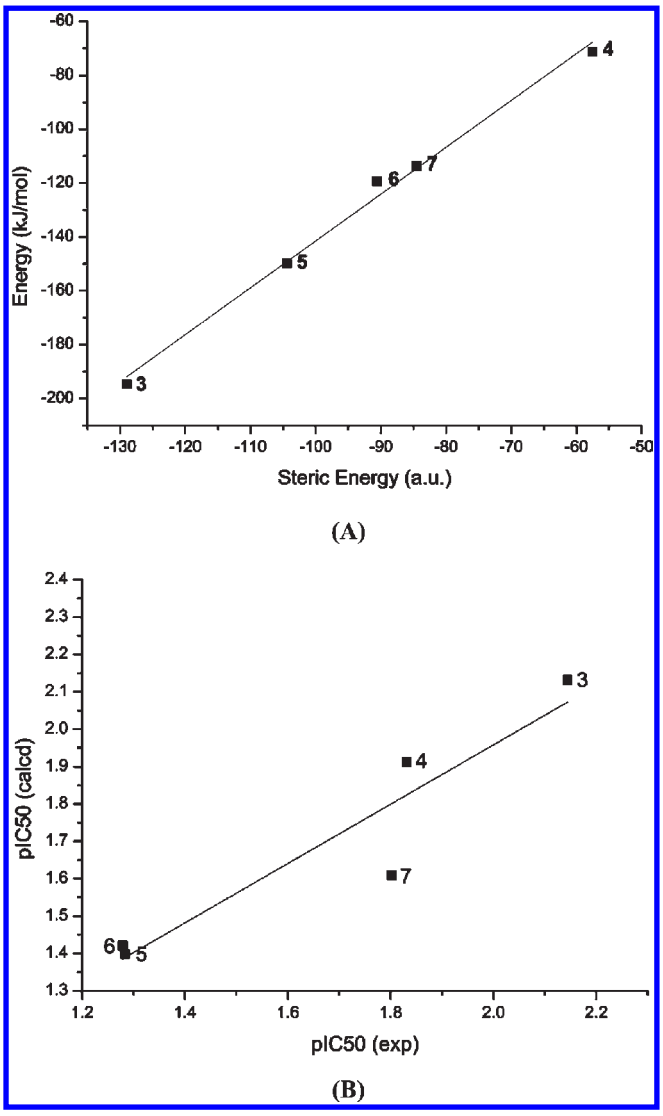

Figure 9. (A) Linear regression graph correlating binding affinity and steric interactions. (B) Correlation between experimental and theoretical inhibitory activity (pIC_{50}).

Table 4. Docking Results

	average binding energies (kJ/mol)		
substrate or inhibitor	**EI**	**ESI**	HOMO − 1 (eV)
linoleic		−100.25 (**ES**)	
6	−90.61	−91.66	−3.54
5	−104.43	−83.82	−4.38
3	−129.01	−130.02	−4.53
4	−57.53	−51.24	−6.26
7	−84.52	−58.41	−5.99

and the corresponding binding energies when the inhibitors (I), bind for the formation of either **ESI** or **EI** complexes (Scheme 2).

Hydrogen bonding is evident for all complexes with the noticeable exception of **4**. Complex **6** interacts via H-bonds with ASP768, ASN128, THR529, and CYS127, **5** with LYS110, **3** with ASP768 and GLY247, and **7** with ASP768 and THR529. Although there are considerable steric interactions between the poses and the cofactor, the pose binding pocket remains the same. It is generally

Scheme 2

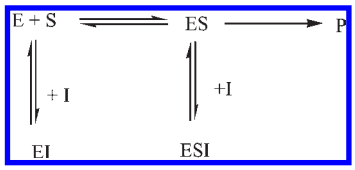

Table 5. Experimental and Calculated **LOX** Inhibition Activity (IC_{50}) of Complexes **3**−**7**

compounds	experimental IC_{50} (μM)	calculated IC_{50} (μM)
3	139.4	135.42
4	67.7	81.5997
5	19.2	24.9582
6	19	26.1639
7	63.4	40.5579

accepted that inhibition action of a compound is directly correlated with the interaction strength between the pose and the macromolecule.[30b] This rule also applies to our case with the noticeable exception of **3**. In order to assess this discrepancy, our theoretical results were evaluated by correlating them with the biological activity of the Sb complexes. Various models had been generated using multivariant linear regression (MLR) and artificial neural networks (ANN) considering biological results (IC_{50}) as the dependent variable. We have found that the best model relating biological activity with the theoretical interaction as expressed by energy terms utilizing MLR is the following (r = 0.957):

$$IC_{50} = 7.90 * \text{“Cofactor(steric)”} + 0.71 * \text{“Pose Energy”} - 2.61 * \text{“Steric Effect”} + 77.08 \quad \text{(V)}$$

The first term is the steric interaction energy between the pose and the cofactors calculated using a LJ12-6 potential approximation, the second is a rough approximation of binding affinity, and the third is the protein steric interaction energy. The importance of the above factors is further confirmed through ANN using the backpropagation method for the training. The relevance scores for the descriptors were 45, 24, and 100, respectively, implying the impact of the steric variables to the successful prediction of the bioactivity model. Table 5 summarizes the experimental and calculated **LOX** inhibition activity (IC_{50}) of complexes **3**−**7**. Figure 9B illustrates the correlation between experimental and theoretical inhibitory activity (pIC_{50}) (R^2 = 0.84; slope = 0.79 ± 0.17). In contrast to our previous work,[30c] the geometrical features for this type of complexes appear to be crucial for the inhibition mechanism. This is an additional evidence of different mechanism of action between Sb(III) complexes **3**−**7** and Sn(IV) complexes studied previously[28,30c] (see also **LOX** activity inhibition, above).

The energy of the frontier molecular orbitals are a measure of electron donor or electron acceptor capacity of a compound and in this sense it plays an important role in various biochemical processes such as charge transfer reactions. Data from Table 4 shows that the absolute energy of HOMO − 1 for the most active compounds is lower compared to the less active ones. This means that the most active molecules comparatively act as better

Table 6. Structure Refinement Details for the Complexes **3**−**7**

	3	**4**	**5**	**6**	**7**
empirical formula	$C_{36}H_{42}I_6N_8O_5S_4Sb_2$	$C_3H_5I_3NS_2Sb$	$C_{24}H_{21}I_6N_3S_6Sb_2$	$C_{13}H_{28}I_3N_6OS_3Sb$	$C_5H_5I_3NSSb$
formula weight	1799.88	620.64	1548.70	870.95	612.60
T (K)	100(2)	293(2)	293(2)	293(2)	100(2)
cryst syst	triclinic	triclinic	monoclonic	orthorhombic	monoclinic
space group	$P\bar{1}$	$P\bar{1}$	Cc	$Pbca$	$P2_1/c$
a (Å)	9.1356(2)	8.171(1)	21.923(4)	16.772(3)	7.6079(1)
b (Å)	9.3951(2)	8.849(1)	10.545(2)	16.658(3)	13.5724(3)
c (Å)	15.7122(3)	9.635(2)	17.474(3)	19.232(3)	11.7380(3)
α (deg)	88.6697(17)	104.75(1)	90	90	90
β(deg)	79.1952(18)	111.44(1)	103.95(2)	90	100.368(2)
γ(deg)	86.1677(18)	97.63(1)	90	90	90
V (Å^3)	1321.63(5)	607.02(16)	3920.5(12)	5373.2(16)	1192.25(4)
Z	1	2	2	8	4
ρ_{calcd} (g/cm^3)	2.284	3.396	2.624	2.153	3.419
μ (mm^{-1})	4.732	10.191	6.444	4.722	10.207
$\theta_{min} < 2\theta < \theta_{max}$	$3.1 < 2\theta < 25.0$	$2.4 < 2\theta < 25.0$	$1.9 < 2\theta < 25.0$	$2.1 < 2\theta < 25.0$	$3.1 < 2\theta < 25.0$
data collected	17811	2547	7482	4985	7605
independent reflections (R_{int})	4640 (0.0296)	2080 (0.0635)	6688 (0.1584)	4655 (0.0292)	2092 (0.0464)
R_1, wR_2 [$I > 2\sigma(I)$], S	0.021, 0.0467, 0.97	0.040, 0.0878, 1.03	0.080, 0.1853, 0.99	0.052, 0.1309, 1.07	0.026 0.0507, 0.90

reducing agents for the redox inhibition reactions and further support the importance of HOMO-1 as electron donor.[31]

Conclusions

Antimony(III) iodide complexes with thioamide ligands studied in this work are found to be monomers (**6**), dimers (**3**, **5**) or polymers (**4**, **7**) with either octahedral (**6**) or pseudo-octahedral (**3**, **4**, **5**, and **7**) geometries. Dimers (**3**, **5**) are built up on monomeric units (SbI_3S_2) with square pyramidal geometry where the equatorial ligands are in *trans*-S, *trans*-I arrangement, bridged together through μ_2-I (**3**) or μ_2-S and μ_2-I (**5**) bridges. The *trans*-S, *trans*-X (X = Cl, Br, I) arrangement of the equatorial ligands in case of SbX_3S_2 monomeric units with SP geometry around the metal ion is found to lead to dimeric Sb(III) complexes,[6−8] while *cis*-S, *cis*-X, or *b*,*c*,*d*-X, SP conformations lead to polymeric assemplies. However, in the case of antimony(III) iodide complexes (**4**, **7**), polymeric assemplies could also be built up on monomeric units (SbI_3S) with pseudotrigonal-bipyramidal geometries.

The complexes showed moderate cytostatic activity against several tumor cell lines with a marked preference for human cervix carcinoma (HeLa) cells as it was also observed in the case of the corresponding antimony chloride and antimony bromide complexes.[7,8] However, antimony(III) bromide complexes showed lower activity than the corresponding chlorides and iodides studied, while antimony(III) chloride complexes show comparable activity with that of the corresponding iodides (Table 2).[7,8]

The influence of complexes **3**−**7** on the oxidation of the linoleic acid by the enzyme **LOX** was also in vitro and computationally studied. The neutral Oh mer-S,I-{[SbI_3-(tHPMT)$_3$]·MeOH} (**6**) and the ψ-Oh [(NMeMBZT)-$SbI_2(\mu_2\text{-}I)_2(\mu_2\text{-}S\text{-}NMeMBZT)SbI_2$ (NMeMBZT)] (**5**) complexes inhibit stronger **LOX** oxidation activity with an uncompetitive type of enzyme inhibition. However, their antiproliferative activity does not correspond to the regularity of inhibition of the lipoxygenase activity which was found previously, for tin complexes.[28a−c] This may be due to a different mechanism of action of Sb(III) complexes as compared with the corresponding tin ones.

Computational studies showed that the best model relating biological activity with the theoretical interaction as expressed by energy terms utilizing MLR is given in eq 5. This equation contains: (i) a term for the steric interaction energy between the pose and the cofactors calculated; (ii) a term for the binding affinity; and (iii) a term for the protein steric interaction energy. Furthermore, calculated IC_{50} from eq 5 are correlated with experimental inhibitory activity linearly (Table 5, Figure 9B). In contrast to our previous work for organotin(IV) compounds,[30c] the geometrical features for this type of complexes appear to be crucial for the inhibition mechanism, supporting further our hypothesis of different antitumor activity mechanism of Sb(III) toward organotin-(IV) complexes.

Experimental Section

Materials and Instruments. All solvents used were of reagent grade. Antimony(III) iodide (Aldrich) as well as thiones 2-mercapto-1-methylimidazole (Sigma), 2-mercaptobenzimidazole (Merck), 5-ethoxy-2-mercapto benzimidazole (Aldrich), 2-mercapto-3,4,5,6-tetrahydro-pyrimidine (Aldrich), 2-mercaptopyridine (Fluka), 2-mercaptothiazolidine (Aldrich), 3-methyl-2-benzothiazolinthion (Aldrich), and 2-mercaptopyrimidine (Aldrich) were used without further purification. Lipoxygenase type 1-B from *Glycine max* (soybean), boric acid, and linoleic acid were purchased from Sigma-Aldrich and were used with no further purification. Elemental analyses for C, H, N, and S were carried out with a Carlo Erba EA MODEL 1108 elemental analyzer. Melting points were measured in open tubes with a STUART scientific apparatus and are uncorrected. The UV−vis spectra were collected in a UV−vis/NIR V570 instrument. Infrared spectra in the region of 4000−370 cm^{-1} were obtained for KBr pellets, whereas far-infrared spectra in the region of 400−50 cm^{-1} were measured for polyethylene discs, with a PerkinElmer Spectrum GX FTIR spectrometer. Micro Raman spectra (64 scans) were recorded at room temperature using a low-power (∼30 mW) green (514.5) mm laser on a Renishaw In Via spectrometer set at 2.0 resolution. Thermal studies were carried out on a Shimadzu DTG-60 simultaneous DTA-TG apparatus, under an N_2 flow (50 cm^3 min^{-1}) at a heating rate of 10 °C min^{-1}.

(31) (a) Molfetta, F. A.; Bruni, A. T.; Honorio, K. M.; da Silva, A. B. F. *Eur. J. Med. Chem.* **2005**, *40*, 329–338. (b) Molfetta, F. A.; Freitas, R. F.; da Silva, A. B. F.; Montanari, C. A. *J. Mol. Model.* **2009**, *15*(10), 1175–1184. (c) Do, E.; Santo, L. L.; Galvão, D. S. *J. Mol. Struct. THEOCHEM* **1999**, *464*, 273. (d) Braga, R. S.; Barone, P. M. V. B.; Galvão, D. S. *J. Mol. Struct. THEOCHEM* **1999**, *464*, 257.

Synthesis and Crystallization of 1−8. A 0.5 mmol portion of the appropriate thiones: methimazole (0.057 g, 0.5 mmol), 2-mercapto-benzimidazole (0.075 g, 0.5 mmol), 5-ethoxy-2-mercaptobenzimidazole (0.097 g, 0.5 mmol), 2-mercapto-thiazolidine (0.059 g, 0.5 mmol), 3-methyl-2-mercaptobenzothiazole (0.090 g, 0.5 mmol), 2-mercapto-3,4,5,6-tetrahydro-pyrimidine (0.058 g, 0.5 mmol), 2-mercaptopyridine (0.055 g, 0.5 mmol), and 2-mercaptopyrimidine (0.056 g, 0.5 mmol) were dissolved in acetonitrile (10 cm^3). A solution of antimony(III) iodide (0.125 g, 0.25 mmol) in methanol (10 cm^3) was then added to the above solutions of all complexes. The resulting solutions were filtered off, and the clear solutions were kept in the dark at room temperature to give crystals of the named **3**−**7** except for **1**, **2**, and **8**, which precipitated as powders. All solid products are stable when kept in darkness at room temperature.

1. Red powder; yield, 65%. Melting point, 105 °C. Elemental analysis, found: C, 14.57; H, 2.15; N, 7.29; S, 9.02. Anal. calc. for $C_9H_{16}I_3N_4OS_2Sb$: C, 14.17; H, 2.11; N, 7.34; S, 8.41. IR (cm^{-1}): 3109 m, 2361 m, 1568 s, 1467 s, 1438 s, 1284 m, 1156 s, 1090 m, 919 w, 738 m, 667 s, 508 m, 403 w.

2. Red powder; yield, 62%. Melting point, 125 °C. Elemental analysis, found: C, 21.12; H, 1.64; N, 7.02; S, 7.83. Anal. calc. for $C_{14}H_{12}I_3N_4S_2Sb$: C, 20.94; H, 1.51; N, 6.98; S, 7.99. IR (cm^{-1}): 3153 m, 2978 m, 1514 s, 1467 s, 1357 m, 1259 w, 1181s, 1032 w, 919 w, 743 s, 711 m, 660 w, 601 m, 481 w.

3. Red crystals; yield, 69%. Melting point, 132 °C. Elemental analysis, found: C, 24.09; H, 2.30; N, 6.19; S, 7.11. Anal. calc. for $C_{36}H_{42}I_6N_8O_5S_4Sb_2$: C, 24.02; H, 2.35; N, 6.23; S, 7.13. IR (cm^{-1}): 3186 m, 2361 m, 1632 s, 1490 s, 1452 s, 1363 m, 1331 w, 1307 s, 1259 m, 1230 m, 1159 s, 1109 m, 1037 m, 982 w, 967 w, 904 w, 842 w, 814 s, 686 m, 627 m, 579 m, 432 m.

4. Red crystals; yield, 57%. Melting point, 154 °C. Elemental analysis, found: C, 5.65; H, 0.72; N, 2.10; S, 10.15. Anal. calc. for $C_3H_5I_3NS_2Sb$: C, 5.80; H, 0.81 N, 2.25; S, 10.32. IR (cm^{-1}): 3256 m, 2362 w, 1510 s, 1454 w, 1336 w, 1302 s, 1041 s, 989 m, 925 m, 655 m, 596 m, 523 m, 425 m.

5. Red crystals; yield, 64%. Melting point, 135 °C. Elemental analysis, found: C, 18.25; H, 1.28; N, 2.51; S, 12.75. Anal. calc. for $C_{24}H_{21}I_6N_3S_6Sb_2$: C, 18.61; H, 1.37; N, 2.71; S, 12.42. IR (cm^{-1}): 3448 m, 2361 s, 1459 m, 1421 m, 1350 s, 1321 m, 1263 m, 1133 m, 1092 s, 1053 m, 977 s, 748 s, 669 m, 634 m, 538 m.

6. Red crystals; yield, 72%. Melting point, 163 °C. Elemental analysis, found: C, 17.54; H, 3.12; N, 9.65; S, 11.15. Anal. calc. for $C_{13}H_{28}I_3N_6OS_3Sb$: C, 17.68; H, 3.20; N, 9.52; S, 10.89. IR (cm^{-1}): 3248 m, 2962 m, 2362 w, 1601 m, 1579 m, 1551 s, 1424 m, 1362 s, 1315 s, 1213 s, 1071 m, 1011 w, 939 w, 810 m, 679 m, 608 m, 415 m.

7. Red crystals; yield, 59%. Melting point, 138 °C. Elemental analysis, found; C, 9.40; H, 0.79; N, 2.21; S, 5.25. Anal. calc. for $C_5H_5I_3NSSb$: C, 9.79; H, 0.82; N, 2.28; S, 5.23. IR (cm^{-1}): 3449 m, 3171 m, 3115 m, 3073 m, 2361 m, 1600 m, 1576 s, 1510 s, 1441 m, 1359 m, 1261 s, 1223 w, 1163 m, 1122 m, 1078 w, 1038 w, 889 w, 836 w, 750 s, 722 m, 486 m, 432 m.

8. Red powder; yield, 52%. Melting point, 151 °C. Elemental analysis, found; C, 13.52; H, 1.20; N, 7.65; S, 8.61. Anal. calc. for $C_8H_8I_3N_4S_2Sb$: C, 13.22; H, 1.11; N, 7.71; S, 8.82. IR (cm^{-1}): 3449 m, 3057 w, 2361 s, 1617 m, 1560 s, 1421 m, 1374 s, 1334 m, 1242 w, 1175 s, 803 w, 743 m, 669 w, 652 w, 470 w.

X-ray Structure Determination. Intensity data for the crystals of **3** and **7** were collected on an Oxford Diffraction CCD instrument,[32a] while a Bruker P4 diffractometer diffractometer was used for **4**−**6**, using graphite monochromated Mo radiation (λ = 0.71073 Å). Cell parameters were determined by least-squares refinement of the diffraction data from 25 reflections.[32b,c]

All data were corrected for Lorentz-polarization effects and absorption.[32a,b] The structures were solved with direct methods with SHELXS97[32c] and refined by full-matrix least-squares procedures on F^2 with SHELXL97.[32d] All non-hydrogen atoms were refined anisotropically, hydrogen atoms were located at calculated positions and refined via the "riding model" with isotropic thermal parameters fixed at 1.2 (1.3 for CH_3 groups) times the U_{eq} value of the appropriate carrier atom. Significant crystal data are given in Table 6.

For the crystal structure of complex **6**, the refined absolute structure parameter was 0.67(9), indicating that the structure consists of a mixture of enantiomers with ratio 0.68:0.32. The crystal structure of complex **7** could be refined better (with regard to both the R factors and displacement parameters) if the sulfur atom is defined as disorder over two position S1/S1A (85/15).

Supplementary data are available from the CCDC, 12 Union Road, Cambridge CB2 1EZ, U.K., (e-mail: deposit@ccdc.cam.ac.uk), on request, quoting the deposition nos. CCDC-740034 (**3**), 744837 (**4**), 744838 (**5**), 744839 (**6**), and 740035 (**7**), respectively.

Computational Studies. The three dimentional coordinates of lipoxygenase were obtained through the Protein Data Bank. (www.rcsb.org/pdb). All solvent molecules within the protein structure were removed from the docking procedure. Molecular docking was performed with the grid based version of the MolDock Score function[29a] as this is implemented in Molegro Virtual Docker software (www.molegro.com). Prior to docking, ground state optimizations on the X-ray structures of the complexes were carried out using the PM3 parametrization scheme[33a] in order to confirm that no significant divergence in the conformations of the complexes due to crystal packing effects. The docked derivatives were scored and reranked using the "reranking score" scheme, and the Molegro Data Analyzer was employed for the theoretical models.

To obtain reliable molecular orbital energies, DFT/B3LYP single point quantum chemical calculations with the split-valence 2-31G* basis set, were performed for the PM3-optimized complexes using GAUSSIAN-03W software package.[33b]

Lipoxygenase Activity Inhibition. LOX inhibitory activity was determined spectrophotometrically by measuring the increase in absorbance at 234 nm for the oxidation of linoleic acid.[28] The reaction mixture contained (final concentration) the test compounds, dissolved in DMSO at concentrations of 5−300 μM, or the solvent (control) and linoleic acid 300 μM, in borate buffer (pH = 9.0). The total sample value was 3 cm^3. The reaction was started by adding a lipoxygenase in amount of 500 units for every 3 cm^3 of reaction mixture. Six different concentrations of each complex were used for the inhibition activity experiments. The increase in absorbance was recorded every 1 s during 10 min under controlled temperature 25 °C.

The kinetic constants of **LOX** activity were measured under standard assay conditions using linoleic acid concentrations ranging from 10 to 1000 μM in the presence of constant concentration of the complex or DMSO (solvent). The respective kinetic parameters were evaluated by plotting the data on a Lineweaver−Burk double reciprocal graph. Every experiment was repeated three times.[28]

Cytostatic Activity Assays. Murine leukemia L1210, murine mammary carcinoma FM3A, human T-lymphocyte Molt 4, and CEM and human cervix carcinoma HeLa cells were suspended at 300 000−500 000 cells mL^{-1} in RPMI-1640 culture medium supplemented with 10% fetal bovine serum and 2 mM L-glutamine, and 100 μL of the cell suspensions were added to 100 μL of an appropriate dilution of the test compounds in 96-well-microtiter plates. After incubation at 37 °C for two (L1210 and FM3A) or three (Molt4, CEM and HeLa) days, the cell number was determined using a Coulter counter. The number of the suspension cells could be counted directly; the number of the monolayer HeLa cells were counted after detachment of the cells upon trypsinization. The IC_{50} was defined as the compound concentration required to inhibit cell proliferation by 50%.

Acknowledgment. This research was carried out in partial fulfilment of the requirements for the Ph.D. thesis of I.I.O., under the supervision of S.K.H., at the University of Ioannina. S.K.H., N.H., E.R.M, and I.S.B. would like to acknowledge a NATO grant for the exchange of scientists (PDD(CP)-(CBP. NR.NRCLG 983167). I.I.O. would like to thank the Hellenic Ministry of Education for a scholarship for postgraduate studies. E.R.M acknowledge RFBR (09-03-00090); Program "Biomolecular and Medicinal Chemistry" of RAS. The research of J. B. was supported by grant GOA no. 05/19 of the K.U. Leuven.